International Journal of Latest Engineering and Management Research (IJLEMR)
ISSN: 2455-4847
www.ijlemr.com || REETA-2K16 ǁ PP. 01-16

Control Scheme With Voltage Support Capability Under Voltage Sags for Distributed Generation Inverters

M.D.BADRINATH[1], M.LOKANADHAM[2]
[1]*PG student, Department of Electrical & Electronics Engineering, S.V.P.C.E.T, PUTTUR*
[2]*Associate professor, Department of Electrical & Electronics Engineering, S.V.P.C.E.T, PUTTUR*

Abstract: Voltage sags are one of the main problems in trans- mission and distribution grids with high penetration of distributed generation. This paper proposes a voltage support control scheme for grid-connected power sources under voltage sags. The control is based on the injection of reactive current with a variable ratio between positive and negative sequences. The controller determines, also, the amount of reactive power needed to restore the dropped voltage magnitudes to new reference values confined within the continuous operation limits required in grid codes. These reference values are chosen in order to guarantee low current injection when fulfilling the voltage support objective. Selected experimental results are reported in order to validate the effectiveness of the proposed control.

Keywords: Distributed generation, low-voltage ride-through (LVRT), reactive power injection, voltage sag.

INTRODUCTION

The number of distributed energy sources connected to the public grid is increasing significantly due to the deregulation of the electric power distribution industry and to environmental issues. The connection of a large amount of distributed generation sources(DGS) over the entire transmission and distribution systems can lead to instability when electrical disturbances appear in the grid. One of the most challenging disturbances in the transitory reduction of the rms voltage in one or more grid phases, which is known as voltage sag. There exist some international standards and different national grid codes that regulate the behavior of grid connected power sources in nominal conditions and also under voltage sags. The basic grid code requirements under voltages are two: setting the point of common coupling (PCC) voltages within the limits for continuous operation, known as low-voltage ride-through(LVRT), and fixing the amount of reactive current injection.

Now a days, the transmission system voltage is supported by conventional high-rated power plants via synchronous generators and hardware compensators in the semiconductor technologies, different voltage-sourced converters are being used to improve the electric power system: Active filters, static synchronous static synchronous compensators,etc.. Thanks to these advances, an ancillary functionality of the low and medium-rated DGS is to control the reactive current injection in order to support the PCC voltages during voltage sags. Reactive power injection is normally done via positive sequence, which raises the positive voltage sequence, but leaves the negative voltage sequence unchanged. Then, in case of unbalanced sags with one or two dropped phases, the conventional strategy of equal increase in all PCC phase voltages can lead to surpassing the maximum allowable voltage magnitude, and causing the system disconnection from the grid. Recently, some works have dealt with the injection of reactive power via positive and/or negative sequences , the voltage support control is based on PI controllers, with the drawback of having to tune these controllers to handle a wide range of voltage imbalances. In a bulky series-parallel two-module system is used to feed critical loads that require high-quality voltage. Studies deal with the mitigation of dc-link voltage fluctuations in DGS due to grid imbalances but not with the PCC voltage support. In a flexible reactive current injection scheme during voltage sags is proposed that provides PCC voltage raising and equalizing by injecting reactive current via both positive and negative sequences. However , the work is only a preliminary study, since the raising and equalizing of the phase voltages is done without a voltage loop.

This paper proposes a voltage controller under voltage sags based on the current scheme presented,which restores the dropped voltages to its continuous operation limits, thus guaranteeing LVRT and also increasing the stability of the power system. A detailed mathematical analysis of the injected currents during the voltage sag is carried out in order to develop the proposed control. The control objective is accomplished when the proper values of both the reactive power reference and the variable ratio between positive and negative sequence reactive current are set. These control parameters are calculated online using a simple algorithm based on the line impedance knowledge. Selected experiments with several types of voltage sags are reported in order to evaluate the performance of this control scheme.

The paper is organized as follows. Section II describes the grid-connected DGS system, analyzes the PCC voltages and inverter currents under voltage sags, and describes the grid code requirements that must be applied under these disturbances. Section III proposes the voltage support scheme based on the injection of

positive and negative sequence reactive power. Section IV corroborates the expected features of the proposed controller by means of selected experimental results. Section V presents the conclusions of this study.

II GRID-CONNECTED INVERTERS UNDER VOLTAGE SAGS

This section begins with the description of grid-connected DGS. Then, the voltages at the PCC under voltage sags are mathematically characterized, giving a general classification of these faults. Later the grid code requirements under voltage sags are described. Finally, the expressions of active and reactive currents injected by the DGS during the voltage sag are given.

A. Grid-Connected Three-Phase Inverter

Fig. 1 shows the diagram of a DGS connected to the grid through a three-phase three-wire inverter. In this configuration a large dc-link capacitor is placed for decoupling the power source module and the utility. The inverter is connected to the PCC through an *LCL* filter. When the system is connected to the grid via a mainly inductive line, the mains can be modeled with an inductance *Lg* in series with a three-phase voltage source **vg** . An external voltage controller is responsible for obtaining the voltage reference for the dc-link that guarantees optimum power generation in the DGS. The output of this controller provides the active power reference value $P*$ related to the active power that must be injected to the grid. The design and analysis of this external dc-link loop has been widely described in the literature and, therefore, will not be considered here. When the system is in continuous operation mode, the control block shown in the figure will drive the inverter switches in order to inject the generated power to the grid. To accomplish this objective, the PCC voltage **v** and the inverter current **i** must be sensed.

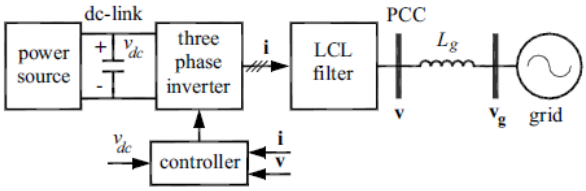

Fig. 1. Diagram of a three-phase inverter connected to the grid.

B. Sag Classification and Characterization

When voltage disturbances occur in the grid, the PCC voltage is also affected, and the control performance is deteriorated. Thus, the PCC voltage behavior under voltage sags must be characterized appropriately.

1) Sag Classification: The causes of the voltage sags are mainly short circuits between phases or between phases and ground, overloads, startup of motors, etc. The nature of the sag mainly depends on fault type (phase to ground, phase to phase, etc.), system grounding and fault location . Independently of the fault type and location, the sag can be characterized by its signature at the PCC. A simplified sag classification can be done according to the number of dropped phase-to-neutral voltages: single phase (type I), double phase (type II), and three phase (type III).

2) Sag Detection and Characterization: The instantaneous PCC voltages during a sag can be described as the addition of positive, negative, and zero symmetric sequences. Taking into account that in three-wire systems zero voltage sequences are not present, the instantaneous PCC phase voltages can be expressed in the stationary reference frame (SRF) as a function of time as

$$v_\alpha = v_{\alpha p} + v_{\alpha n} = V_p \cos(\omega t + \delta_p) + V_n \cos(\omega t + \delta_n) \quad (1)$$

$$v_\beta = v_{\beta p} + v_{\beta n} = V_p \sin(\omega t + \delta_p) - V_n \sin(\omega t + \delta_n) \quad (2)$$

where $v_{\alpha p}$, $v_{\beta p}$ and $v_{\alpha n}$, $v_{\beta n}$ are the SRF positive and negative voltage sequences, respectively, V_p and V_n are its amplitudes, ω is the grid angular frequency, and the pair δ_p , δ_n are the initial phase angles of positive and negative sequences. In order to simplify the notation, a new variable, the sequence phase-angle, i.e., the phase between positive and negative sequences, can be defined as

$$\delta = \delta_p - \delta_n . \quad (3)$$

Any sag can be characterized and classified if the magnitudes V_p, V_n , and δ are known. These three magnitudes can be calculated online by sensing the phase vector **v** and then using the SRF theory to evaluate the positive and negative sequences of the space vector. There are different techniques to evaluate the space vector

sequences, and among them, one promising detection algorithm . Afterward, since the voltage vector sequences are known, the amplitudes of the positive and negative sequences and the phase angle can be calculated online using

$$V_p = \sqrt{v_{\alpha p}^2 + v_{\beta p}^2} \quad (4)$$

$$V_n = \sqrt{v_{\alpha n}^2 + v_{\beta n}^2} \quad (5)$$

$$\delta = \cos^{-1}\left(\frac{v_{\alpha p}v_{\alpha n} - v_{\beta p}v_{\beta n}}{V_p V_n}\right). \quad (6)$$

From (1) and (2), the module of the natural frame phase voltages can be written as a function of *Vp*, *Vn* and the phase angle δ as

$$V_a = \sqrt{V_p^2 + V_n^2 + 2V_pV_n\cos(\delta)} \quad (7)$$

$$V_b = \sqrt{V_p^2 + V_n^2 + 2V_pV_n\cos(\delta - {}^2/_3\pi)} \quad (8)$$

$$V_c = \sqrt{V_p^2 + V_n^2 + 2V_pV_n\cos(\delta + {}^2/_3\pi)} \quad (9)$$

where *Va*, *Vb* , and *Vc* are the amplitudes of the PCC phase voltages. These expressions will be used later to develop the control proposal of this study.

Keeping in mind the previous analysis, any voltage sag can be detected and characterized using (4)–(6). In a balanced system the negative sequence is zero, and the positive sequence coincides with the phase voltage amplitudes. Type III sags are characterized by an equal drop in the three PCC phase voltages,
consequently, only the positive sequence is present. Conversely, if the negative sequence is present, by measuring the phase angle δ the sag type (I or II) and the dropped phases are easily derived. Fig. 2 shows the sequence phase angle that determines the sag type and the dropped phase(s). It must be noted that in transmission and distribution systems the majority of the voltage sags have a sequence phase angle, which is roughly an integer multiple of $\pi/3$ rad, i.e., $\delta = n \cdot \pi/3$ rad, $n \in N$. For example, if the sequence phase angle is $\delta = \pi/3$ rad, the sag type is I with a voltage drop only in phase *b*.

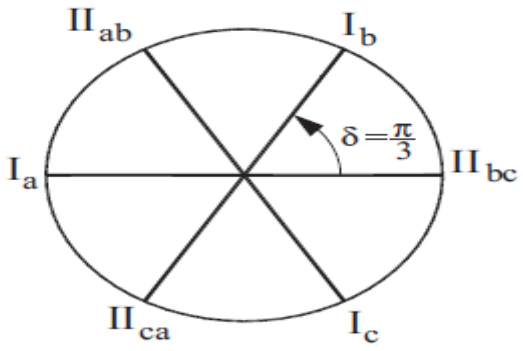

Fig. 2. Sag characterization based on the sequence phase angle δ. Uppercase letters denote the sag type (I or II), and lowercase letters denote the dropped phase(s).

C. Grid Code Requirements Under Voltage Sags

The main objective of a grid-connected DGS is to deliver the generated power to the grid even during voltage sags. Additionally, wind grid codes require also some amount of reactive current injection during voltage sags in order to support the transmission or distribution system. The amount of reactive current that must be injected depends on the sag depth and its time duration. Under the point of view of LVRT protocols, national grid codes and international standards establish the limits of continuous operation voltages at the PCC. These limits range from a minimum voltage of 0.85 per unit (p.u.) of the rms base voltage to a maximum value of 1.1 p.u. Then, for continuous operation, the natural frame voltage amplitudes (7)–(9) must fulfill

min (*Va*, *Vb*, *Vc*) ≥ 0.85 (10)

max (*Va*, *Vb*, *Vc*) ≤ 1.1 (11)

When a voltage sag occurs and the minimum limit is underpassed (or the maximum limit is overpassed) by one or more phase voltages, the DGS must be disconnected from the grid after the established trip time.

D. Current Injection During Voltage Sags

According to the instantaneous power theory, the active power *p* and reactive power *q* injected to the grid by a three phase DGS can be defined as

$$p = \frac{3}{2}(v_\alpha i_\alpha + v_\beta i_\beta) \quad (12)$$

$$q = \frac{3}{2}(-v_\beta i_\alpha + v_\alpha i_\beta). \quad (13)$$

Based on these expressions, the reference currents can be derived ensuring that the instantaneous powers follow their references, $p = P^*$ and $q = Q^*$

$$i_\alpha^* = i_\alpha^*(p) + i_\alpha^*(q) \quad (14)$$

$$i_\beta^* = i_\beta^*(p) + i_\beta^*(q) \quad (15)$$

where the active currents are

$$i_\alpha^*(p) = \frac{2}{3}\frac{v_{\alpha p}}{V_p^2}P^* \quad (16)$$

$$i_\beta^*(p) = \frac{2}{3}\frac{v_{\beta p}}{V_n^2}P^* \quad (17)$$

and the reactive currents are

$$i_\alpha^*(q) = \frac{2}{3}\frac{k_q v_{\beta p} + (1-k_q)v_{\beta n}}{k_q V_p^2 + (1-k_q)V_n^2}Q^* \quad (18)$$

$$i_\beta^*(q) = -\frac{2}{3}\frac{k_q v_{\alpha p} + (1-k_q)v_{\alpha n}}{k_q V_p^2 + (1-k_q)V_n^2}Q^*. \quad (19)$$

The control scheme for active power injection, (16) and (17), provides a current that follows the averaged positive voltage sequence. It avoids the appearance of current harmonics when the grid presents unbalanced voltages, at the expense of generating oscillations in the injected active power at twice the grid frequency. The control scheme for reactive currents (18) and (19) and provides flexible positive/negative reactive power injection. Also, with this scheme no harmonic distortion is introduced by the injected reactive currents. The control balancing factor *kq* allows to flexibly inject the reference reactive power *Q** via positive and negative sequences, simultaneously. The parameter *kq* can take values inside the range $0 \leq kq \leq 1$. When *kq* tends to 1, the reactive current is injected via positive sequence, and when *kq* tends to 0 it is injected via negative sequence. The main contribution of the previous work was a new current scheme, (18) and (19), for injecting reactive power and the qualitative analysis of its influence in the positive and negative PCC voltage sequences during a voltage support scenario. The values of the control parameters *Q** and *kq* were chosen in an open loop, without any knowledge or control about the new PCC voltage values after the reactive current injection. Then, to complete that work, it would be interesting to develop a novel voltage control scheme to inject both the correct amount (determining *Q**) and the accurate balance (determining *kq*), of reactive current that bring the PCC voltages inside the continuous operation limits. This way, in Section III, a closed loop voltage control scheme based on the current scheme is developed to provide online values for *Q** and *kq* depending on the sag profile and grid characteristics.

III. PROPOSED VOLTAGE SUPPORT CONTROL SCHEME

The main purpose of this study is to develop a voltage support method that diminishes the adverse effects of sags in the PCC voltage, i.e., avoid under voltage and also overvoltage. In an inductive grid, the injection of reactive current will produce a positive increment in the PCC voltages. During a voltage sag, the DGS disconnection could be avoided if the amount of injected reactive current increases the PCC voltages sufficiently to bring them within the continuous operation limits.

A. PCC Voltage Reference Values for Continuous Operation

Fig. 3 shows three examples of voltage sags measured at the PCC, as well as the proposed voltage reference values that guarantee continuous operation. Two dashed lines, one at 1.1 p.u. and another at 0.85 p.u. are drawn horizontally to highlight the operation boundaries. The difference between continuous operation boundaries is a constant value

$\Delta V\text{boundaries} = 1.1 - 0.85 = 0.25$ p.u. (20)

and the difference between the amplitudes of the PCC voltages during the sag is defined as

$\Delta V = \max(Va, Vb, Vc) - \min(Va, Vb, Vc)$. (21)

These two quantitieswill be used to determine the appropriate control strategy depending on the sag profile.
Fig. 3(a)(left) shows the rms phase amplitudes of a type I sag with $\Delta V < \Delta V$boundaries . In Fig. 3(a) (right) the reference amplitude for the droped phase *Vc** is set to be the low boundary value, *VL**= 0.85 p.u., and the reference amplitudes for the other phase voltages, *Va** ∗ and *Vb** are set to *VH** = (0.85 + ΔV)p.u.

Implementing a control strategy that injects only positive sequence reactive current will raise the three phase voltages equally [23]. Then, when the amplitude *Vc* reaches its referenc*Vc** the other two phase amplitudes, *Va* and *Vb* , will remain below 1.1 p.u., i.e., within the operation boundaries. Fig. 3(b)and (c) shows the PCC phase voltages (left) and its references(right) during type II with $\Delta V < \Delta V$boundaries and during type III sags. As can be seen, the reference values are chosen as

min (*Va, Vb, Vc*) = *VL**= 0.85 (22)

max (*Va, Vb, Vc*) = *VH** = 0.85 + ΔV. (23)

Obviously, one could chose to place the reference values for these voltage sags in any position within the 0.85 to 1.1p.u. range; for example, high and low references set to the nominal voltage, (i.e., 1 p.u.). However, in this case, the amount of injected current would be higher than when choosing the proposed values.
Fig. 4(a)(left) shows the phase amplitudes of a type I voltage sag with $\Delta V \geq \Delta V$boundaries and Fig. 4(a)(right) shows its reference amplitudes. In this case, if an equal rise in the three phases is produced, the phase amplitudes *Va* and *Vb* will exceed the maximum operation limit. Then, a second control strategy is necessary to increase and also to equalize the three phases in order to guarantee the allocation of the PCC voltages within the boundaries. This will be done by injecting both positive and negative sequence reactive current [23]. Fig. 4(b) shows the PCC phase voltages (left) and its references (right) during a type II voltage sag with $\Delta V \geq \Delta V$boundaries.

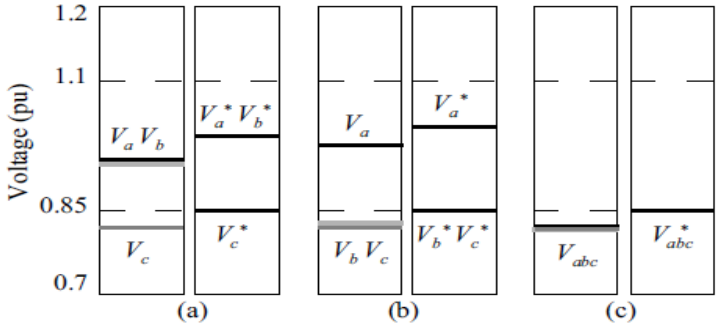

Fig. 3. Examples of voltage sags with $\Delta V < \Delta V$boundaries . (a) Type I;(b) Type II; (c) Type III. (left) PCC phase voltages during the sag. (right) Proposed phase voltage reference values.

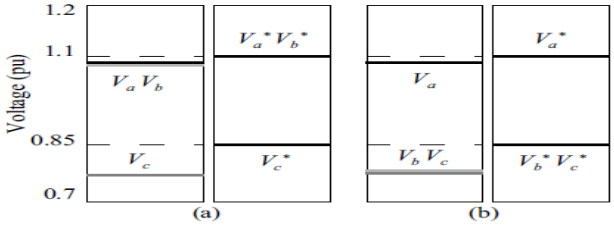

Fig. 4. Examples of voltage sags with $\Delta V \geq \Delta V$boundaries . (a) Type I;(b) Type II. (left) PCC phase voltages during the sag. (right) Proposed phase voltage reference values.

In both cases, the low reference value coincides with (22) and the high reference value is saturated to the boundary high value

max (*Va, Vb, Vc*) = *VH** = 1.1. (24)

Also in these two last cases, the reference values are chosen to minimize the reactive current injection.With these objectives in mind, in the five cases of voltage sags presented the voltage reference profiles are defined as shown in Figs. 3 and 4.

Once the PCC voltage reference amplitudes in the natural frame are chosen, it would be useful to transform them to positiven and negative sequence values. So, (7)–(9) can be solved for sag types I and II by equating the minimum phase amplitude to 0.85 p.u. and the maximum to 0.85 + ΔV p.u. (saturated to1.1 p.u.), obtaining the reference values for positive V_{p^*} and for negative sequence *Vn**

Type I:
$$V_p^* = \frac{1}{2}V_H^* + \frac{1}{6}\sqrt{12(V_H^*)^2 - 3(V_L^*)^2} \quad (25)$$
$$V_n^* = \frac{1}{2}V_H^* - \frac{1}{6}\sqrt{12(V_H^*)^2 - 3(V_L^*)^2} \quad (26)$$

Type II:
$$V_p^* = \frac{1}{2}V_L^* + \frac{1}{6}\sqrt{12(V_L^*)^2 - 3(V_H^*)^2} \quad (27)$$
$$V_n^* = -\frac{1}{2}V_L^* + \frac{1}{6}\sqrt{12(V_L^*)^2 - 3(V_H^*)^2}. \quad (28)$$

For type III, the sequence reference values are directly

Type III:
$$V_p^* = 0.85 \quad (29)$$
$$V_n^* = 0. \quad (30)$$

B. Derivation of Control Parameters Q* and kq:

When a current **i** flows from the DGS into the grid, it produces a voltage increment in the line inductance that could bring the PCC voltages within the continuous operation boundaries, see Figs. 3 and 4. The voltage support protocol must determine the injected reactive current necessary to guarantee continuous operation. The basic steps of the proposed voltage support algorithm are the following:

1) Detect and characterize the sag, using the online evaluation of (4)–(6);
2) Set the positive and negative voltage sequence reference values (25)–(30) according to both the sag type, and the natural frame reference values (22)–(24);
3) And, finally, find the parameter values*Q** and *kq* to be used in (18) and (19) in order to generate the currents that raise the PCC voltages to the previously established limits. In order to determine the currents that fulfill the voltage support protocol it is necessary to estimate which is the effect of the current over the line inductance. Then, the value of the line inductance must be roughly known. In order to simplify the analysis, only reactive current injection is assumed: *P** = 0 in (16) and (17). In Section IV, both active and reactive powers are injected during the voltage sag to demonstrate experimentally that the contribution of the active power to the voltage variation is minimum and can be neglected. Also, it is assumed that the inner current loop is fast enough to ensure that **i** = **i***. After these assumptions, the grid voltage can be expressed as (see Fig. 1)

$$\mathrm{v_g} = \mathrm{v} - L_g\frac{d\mathrm{i}^*(q)}{dt}. \quad (31)$$

By measuring online both the line inductance and the PCC voltage, and knowing the injected current, the grid voltage **vg** can be calculated. With the estimated grid voltage vector, it is easy to calculate the amount of reactive current needed to raise the PCC voltages to their reference values. By inserting (1), (2), (18), and (19) in (31), the SRF grid voltage can be derived as

$$v_{g\alpha} = v_\alpha - \frac{2}{3}\omega L_g\frac{k_q V_p\cos(\omega t) - (1-k_q)V_n\cos(\omega t+\delta)}{k_q V_p^2 + (1-k_q)V_n^2}Q^* \quad (32)$$

$$v_{g\beta} = v_\beta - \frac{2}{3}\omega L_g\frac{k_q V_p\sin(\omega t) + (1-k_q)V_n\sin(\omega t+\delta)}{k_q V_p^2 + (1-k_q)V_n^2}Q^*. \quad (33)$$

Taking separately the positive and the negative sequences of the calculated grid voltages, (32) and (33) results in

$$V_{gp} = V_p - \frac{2}{3}\omega L_g\frac{k_q V_p}{k_q V_p^2 + (1-k_q)V_n^2}Q^* \quad (34)$$

$$V_{gn} = V_n + \frac{2}{3}\omega L_g\frac{k_q V_n}{k_q V_p^2 + (1-k_q)V_n^2}Q^*. \quad (35)$$

For each sag type, replacing *Vp* and *Vn* in (34) and (35) by their reference values *Vp** and *Vn** [obtained by (25)–(30)], asecond-order equation system results, with unknowns *Q** and *kq* . Then, by solving this system, the control parameters can be derived as

$$Q^* = \frac{3}{2}\frac{V_p^*(V_p^* - V_{gp}) - V_n^*(V_n^* - V_{gn})}{\omega L_g} \qquad (36)$$

$$k_q = \frac{V_n^*(V_p^* - V_{gp})}{V_p^* V_{gn} - V_n^* V_{gp}}. \qquad (37)$$

Using Q^* and kq values expressed in (36) and (37) to implement the reactive reference currents (18) and (19), it is guaranteed that the PCC voltages will reach their reference values.

C. Proposed Voltage Support Scheme

The proposed voltage support control scheme is depicted in Fig. 5. In the first block, the voltage at the PCC is sensed and processed on the basis of the SRF theory with the following steps: 1) detect the voltage sag by comparing the PCC voltages rms values with the lower boundary limit; 2) extract the amplitudes of the positive and negative sequences; 3) determine the sag type; and 4) with these data, set the positive and negative PCC voltage reference amplitudes *Vp** and *Vn**using (25)–(30) with the natural frame reference values (22)–(24).

The second block is responsible for estimating the grid voltage by means of (34) and (35), taking into account that the reactive power reference $Q*$ and the balancing parameter *kq* are given at the output control scheme and *Lg* is properly measured.

The third block calculates the new reactive power reference $Q*$ and *kq* values using (36) and (37). If the rms value of any phase current **i** reaches the maximum rated current, the values of $Q*$ and *kq* are saturated in order to avoid system damage. In this case, the voltage support objective cannot be fulfilled. If the maximum current rating is not exceeded, the new values of $Q*$ and *kq* are calculated and sampled at each line cycle *T* and then used to generate the reactive reference currents (18) and (19). The transient response of the proposed control scheme will be determined basically by the sequence extractor response and the sampling period. By setting the sampling period at one line cycle, a settling time of *ts*~□5·*T* is expected. A lower sampling period is not possible since the voltage sequence extractor requires at least one line cycle to stabilize the sequence amplitudes . The block Diagram of the voltage support control scheme is as shown below fig.5.

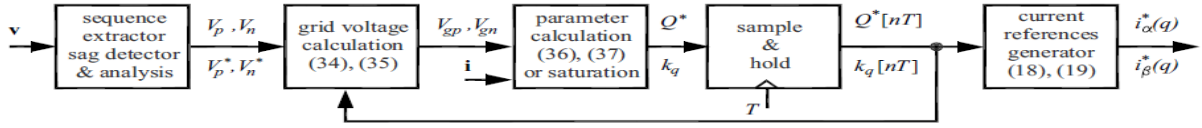

D. Control Strategies for Different Sag Profiles

As stated previously, the control strategy to be chosen will depend on the relation between Δ*V*boundaries and Δ*V*.

1) *Strategy 1*, Δ*V* < Δ*V*boundaries . The three PCC phase voltages must be increased equally. In this case, the reactive current injection must be done only via positive sequence: setting *kq* = 1, i.e., the positive voltage sequence is increased, while the negative voltage sequence is unaffected. Following this strategy, only the control parameter *Q** must be calculated online using (36).

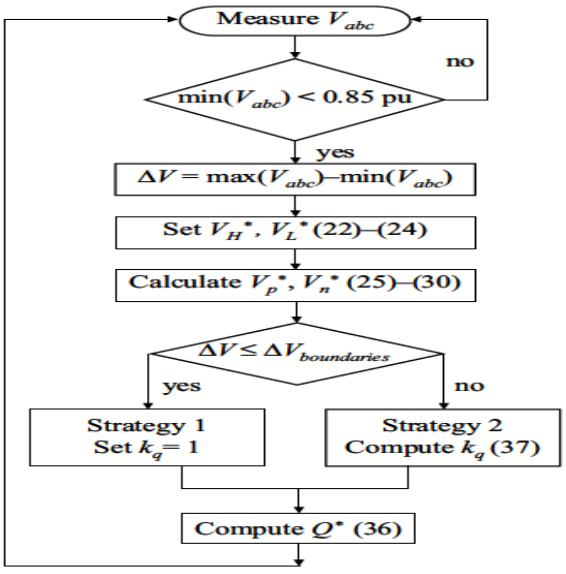

fig.6 Flux diagram of the algorithm, which determines the control strategy under different voltage sags.

2) *Strategy 2,* $\Delta V \geq \Delta V$boundaries . In this case, if *kq* is set to 1 (i.e., equal increment in the three phases) the higher voltage at the PCC will overpass the maximum boundary, thus forcing the disconnection of the DGS after the trip time. To avoid this, the parameter *kq* must be less than 1, allowing some amount of reactive power injection via negative sequence, which tends to equalize the phase voltages. Note that, in this case, both parameters Q^* and *kq* are calculated online using (36) and (37).

The sag detector block in Fig. 5 is also responsible for choosing the adequate strategy for each situation. Fig. 6 shows the flux diagram of the algorithm implemented in order to determine the control strategy to be used.

IV. EXPERIMENTAL RESULTS

An experimental prototype rated at 2.3 kVA was built using a SEMIKRON full bridge as the power converter and a TMS320F28335 floating point digital signal processor as the control platform. The DGS behavior is emulated using an AMREL-SPS1000 dc source. The utility grid is emulated by means of a programmable three-phase Pacific AMX-360 ac source connected to the PCC, with coupling inductors modeling the line inductance (see Fig. 1). The current control consists of an SRF proportional-resonant controller, [33]. A detection system implemented with generalized integrators is used to evaluate the space vector sequences, [29], [34]. Table I lists the parameter values for both the inverter and the controller. Due to the setup low power rating, a high grid inductance value (0.12 p.u.) was intentionally used in order to clearly show the capacity of voltage restoration provided by the proposed control scheme. In a real distribution power system, the capacity of voltage restoration is obviously limited by the power rating and the grid stiffness. Some studies consider that the maximum grid impedance for distribution systems is within the 0.05 and 0.1 p.u. range [24], [35].

Different voltage sags have been programmed in the ac source to evaluate the behavior of the system. The programmed sags will follow the same sequential behavior. First, during 0.2 s, the grid voltages are roughly balanced with the following rms voltages: 1.064, 1.069, and 1.076 p.u. At time t = 0.2 s, the sag occurs and three, two or one voltages drop(s) below 0.85 p.u., which is the minimum limit for continuous operation. Afterward, during 0.2 s (from t = 0.2 to 0.4 s) the sag control is not yet enabled, in order to clearly show the voltage sag profile. Then, at time t = 0.4 s, the voltage support control is enabled and the calculation of the control parameters $Q*$ and *kq* begins by means of (36) and (37). The calculation lasts one line cycle. After this delay, the computed values are used in the reference current generation during the following line cycle. Then, the reactive power injection starts and, as a result, the PCC voltage is supported. Finally, at time t = 0.8 s, both the sag and the reactive current injection are disabled. For the entire duration of the experiments, the inverter maintains an active power injection of P^* = 750W, i.e., it continues to sell the generated power to the grid independently of the sag.

TABLE I
SYSTEM PARAMETERS

nominal rated power (base power)	S_b	2.3 kVA
active power reference	P^*	750 W
nominal grid voltage	V_g	110 V rms
nominal grid frequency	f_o	60 Hz
dc-link voltage	v_{dc}	350 V
LCL inverter side inductances	L_i	5 mH
LCL filter capacitors	C_o	1.5 μF
LCL output side inductances	L_o	2 mH
line inductances	L_g	5 mH
sampling frequency	f_s	10 kHz
switching frequency	f_{sw}	10 kHz

A. Supporting Type III Sags

Fig. 7 shows the PCC phase voltages before, during, and after a type III voltage sag. When the sag takes place, at t = 0.2 s, the three rms phase voltages drop to 0.79 p.u. approximately. As stated previously, with type III sags $\Delta V < \Delta V$boundaries , thus the support strategy consists in an equal raising of the threephase voltages until they reach the minimum limit voltage for continuous operation, i.e., 0.85 p.u. The voltage raise is obtained by injecting the reactive power via positive sequence, *kq* = 1. Between t = 0.2 and 0.4 s, the voltage support control is still not enabled in order to clearly show the sag depth. At time t = 0.4 s, the voltage support control is activated and the calculation ofQ^* begins by means of (36), which will be used in the generation

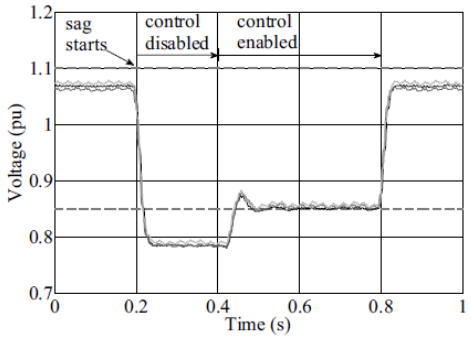

Fig.7 PCC phase voltages during the type III voltage sag.

of the reference currents during the following line cycle. As can be seen, after the control startup, the phase voltages become stabilized at 0.85 p.u. At time t = 0.8 s, the sag disappears and the voltages recover their prefault values.

Fig. 8 shows the measured positive and negative voltage sequences at the PCC, *Vp* , and *Vn* , as well as the estimated grid voltages, *Vgp* and *Vgn* . As can be seen, the value of the positive voltage sequence is increased (in black trace, top figure) when the reactive power is injected via positive sequence. The negative voltage sequence remains unaffected.

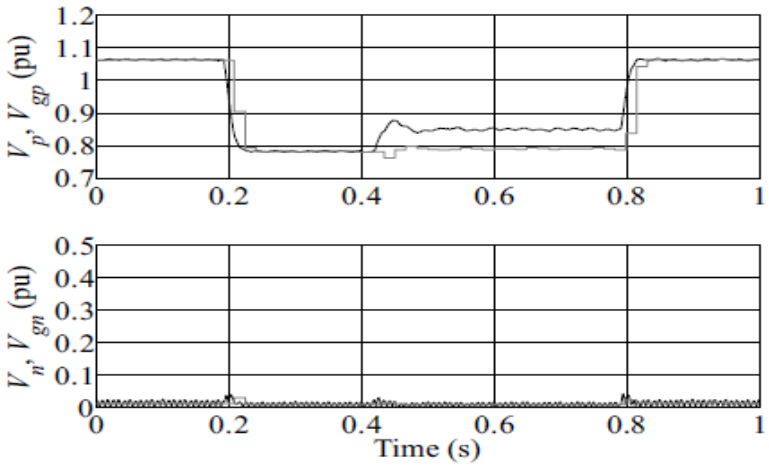

Fig.8 Positive and negative sequence amplitudes(PCC voltages in black grid voltages in gray), type III voltage sag

Fig. 9 shows the computed reactive power reference and the measured reactive power. It clearly shows the stabilization of the calculated reactive power reference, $Q*$ = 1 kVAr. Note that the settling time is approximately 0.1s, as discussed previously(i.e., ts=5 $\cdot T$). The discrete actualization of the computed value $Q*$ at each line cycle can be clearly appreciated in the figure.

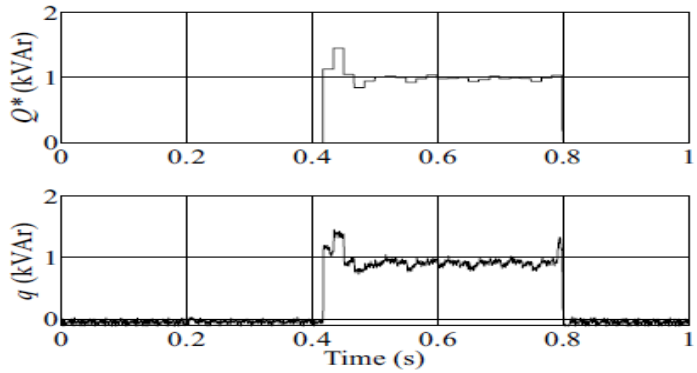

Fig.9 Reactive Power reference and measured reactive power with type III sag.

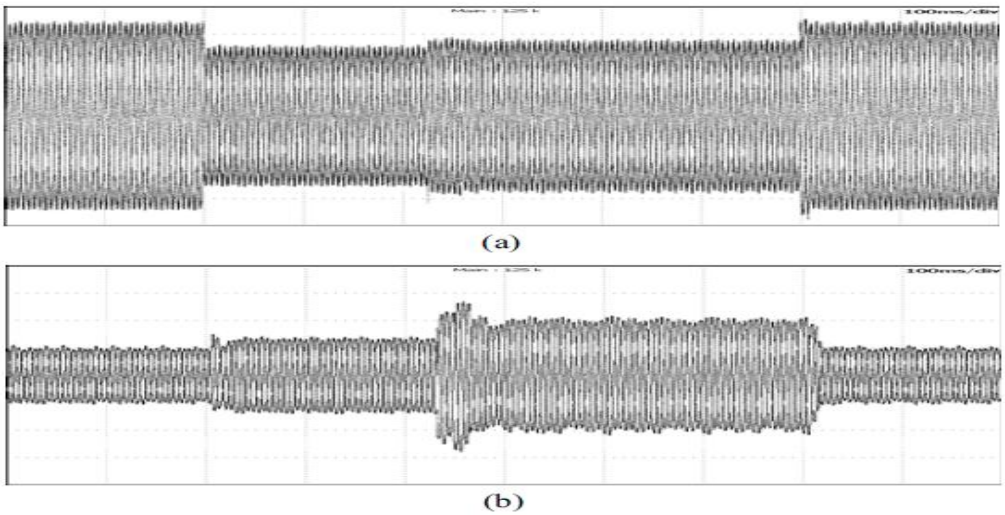

Fig.10. Type III voltage sag, (a)PCC phase voltages(50V/div)and (b) inverter phase currents(2.5A/div),(100ms/div)

Fig. 10 shows the measured instantaneous voltages and currents during the test with sag type III. Before the sag, only active power is injected into the grid. When the sag occurs and the voltage support control is not enabled, an increase in the active current can be observed to maintain the same active power injection. Afterward, when the support control kicks in, the current increment is due only to the reactive power injection. When the sag and the support control cease, the currents return to their initial values, i.e., only active power feeds the grid. Then, the active power generated in the DGS is fed continuously to the grid, without disturbing the voltage support control.

B. Supporting Type II Sags

Fig. 11 shows the PCC phase voltages during a type II voltage sag with $\Delta V < \Delta V$boundaries . In this fault, two of the phase voltages drop to 0.79 p.u. approximately, while the third one drops to 0.91 p.u. In this case, $\Delta V = 0.12$, the reference amplitude voltages are set to $VL^* = 0.85$ p.u. and to $VH^* = 0.97$ p.u. (0.85+0.12), and the calculated positive and negative sequence reference values are $V * p = 0.89$ p.u. and $V * n = 0.08$ p.u. according to (27) and (28). When supporting this sag only the value of Vp is increased, i.e., reactive power is injected via positive sequence. $Q*$ is set automatically to approximately 1 kVAr, with the balancing parameter $kq = 1$. As can be seen, when the control kicks in, the PCC voltages rise to the desired values.

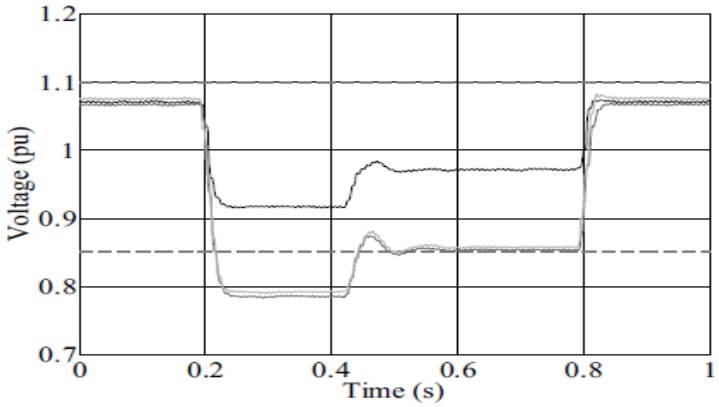

Fig. 11. PCC phase voltages during a type II voltage sag with $\Delta V < V$boundaries .

Fig. 12 shows the PCC phase voltages during a type II voltage sag, now with $\Delta V > V$boundaries . In this fault, two of the phase voltages drop to 0.78 p.u. approximately, while the third one is maintained at 1.071 p.u. The PCC voltage difference is $\Delta V = 0.29$, thus $\Delta V > V$boundaries , and the amplitude reference values are set to $VL^* = 0.85$ p.u. and $VH^* = 1.1$ p.u. (with the calculated references $Vp^* = 0.92$ p.u. and $Vn^* = 0.17$ p.u.). After

the control startup, the two dropped voltages rise to 0.85 p.u., and the nondropped to 1.1 p.u., as desired. In this case, both parameters Q^* and kq are calculated online.

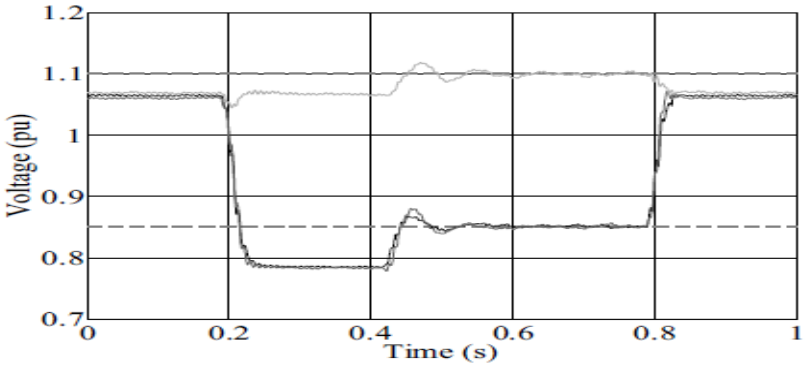

Fig. 12. PCC phase voltages during a type II voltage sag with $\Delta V > V$boundaries

In Fig. 13, the balanced compensation of the PCC positive and negative voltage sequences are clearly shown. As can be seen, the value of Vp is increased (via positive sequence reactive current) and Vn is decreased (via negative sequence reactive current).

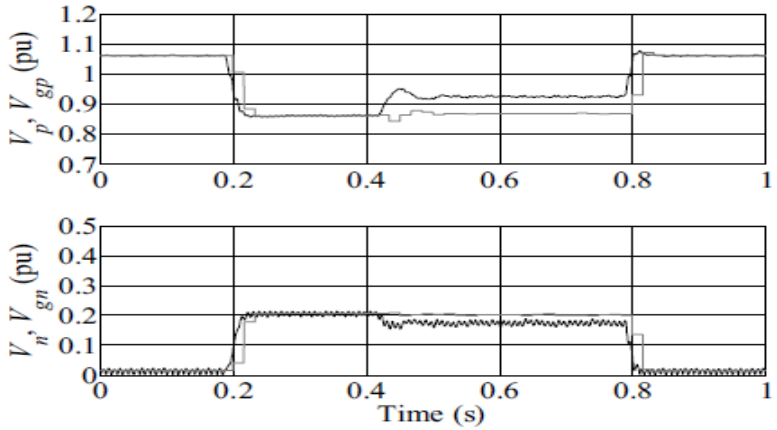

Fig. 13. Sequence amplitudes (PCC voltages in black, grid voltages in gray), type II voltage sag with $\Delta V > V$boundaries .

Fig. 14 shows the control parameter values during this test. Q^* is set automatically to approximately 1.1 kVAr, and the balancing parameter is stabilized at roughly $kq = 0.27$.

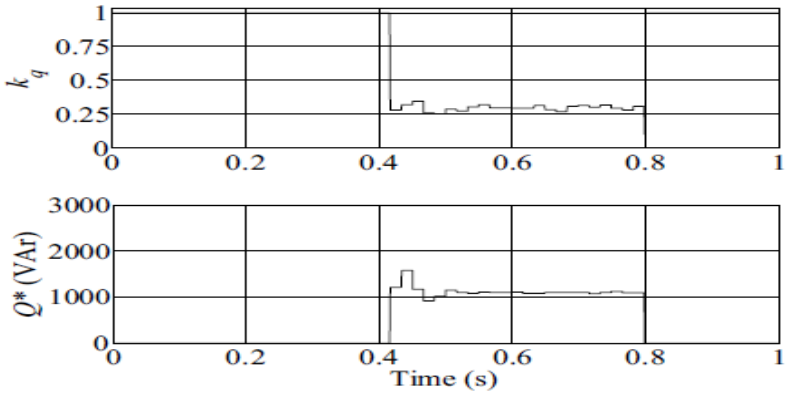

Fig. 14. Control parameter kq and reference value of reactive power Q^*, type II voltage sag, $\Delta V > V$boundaries .

Fig. 15 shows the instantaneous active and reactive power during the type II fault. The mean value of the active power is 750Wfor the duration of the test. The measured mean value of the reactive power is almost 1.1 kVAr, following its reference value, Q^*. When the sag occurs, the system becomes unbalanced, and an oscillation at twice the line frequency appears in both active and reactive power. Note that the apparent power is 1.3 kVA, less than its nominal value Sb , see Table I.

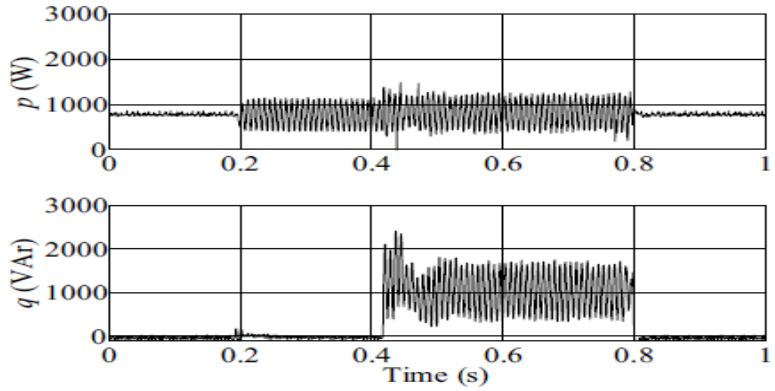

Fig. 15. Measured active and reactive power during the type II voltage sag with $\Delta V > V$boundaries .

C. Supporting Type I Sags

Fig. 16 shows the value of the PCC phase voltages with the programmed type I voltage sag. When the sag occurs, one voltage drops to 0.73 p.u. while the other two voltages drop to 1 pu. The voltage difference is ΔV = 0.27 p.u., thus $\Delta V > \Delta V$boundaries , and the online calculated references are Vp^* =1.01 p.u. and Vn^* = 0.16 p.u. according to (25) and (26). In this test, the reactive power reference value is stabilized at Q^* = 2kVAr approximately, and the balancing parameter is kq = 0.66. As desired, the lower voltage amplitude becomes stabilized to 0.85 p.u., and the other phase amplitudes to 1.1 pu.

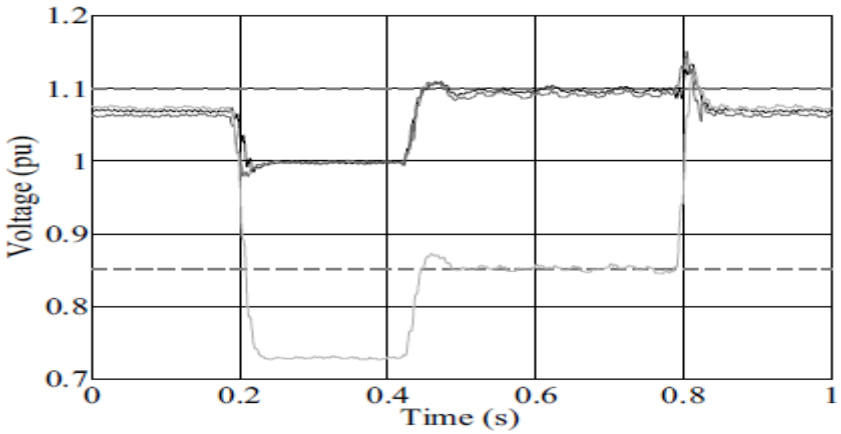

Fig. 16. PCC phase voltages during the type I voltage sag.

D. Supporting Variable Profile Sags

The proposed voltage support control scheme was tested also with a variable profile sag. The idea is to evaluate the control in real conditions with a sag following a slow transient recovery. Fig. 17(a) shows the PCC phase voltages during a type I variable profile voltage sag. Fig. 17(b) shows the PCC phase voltages when the voltage support scheme kicks in just at the beginning of the sag.

Fig. 18 shows the PCC phase voltages during the dynamic sag (top) and when it is corrected (bottom). As can be seen, the control restores the PCC voltages correctly, even in this situation in which the grid voltages are evolving during the sag. Fig. 19 shows the control parameter values during this last test. As predicted, the profile of the control parameters is not constant. At the valley of the sag, Q^* is set by the controller to approximately 2.1 kVAr, a high value due to the depth of the sag. In this case, the maximum delivered apparent power is 2.2 kVA, almost the nominal base value Sb. After t = 0.4 s, the reactive power reference progressively decreases in accordance with the sag profile. Also the balancing parameter evolves with time until it reaches its maximum value, kq = 0.55, at the valley of the sag and after it is reduced to kq = 0.39. As a result, the control continuously adjusts the injection of reactive power by means of positive and negative sequences.

After examining the previous tests, it can be stated that the proposed controller has clearly demonstrated its capability to correct all types of voltage sags. In all the presented tests, the inverter injects less than its maximum acceptable power rating, allowing the system to bring the phase voltages within the continuous operation boundaries. In a real system, however, the capacity of voltage restoration would depend on both the inverter power rating and the grid stiffness.

E. Computational Load

Despite the a priori complexity of the proposed voltage support control scheme, the additional computational load is not excessive. The measured algorithm execution time when the grid operates in normal conditions is 26 μs. This control scheme includes the analog-to-digital converter, the voltage sequence detector, the current reference generator, the current loop, and the modulator. During the sag (when the voltage support algorithm is activated), the execution time suffers an increase of 8 μs, resulting in an idle time of 66% of the sampling period.

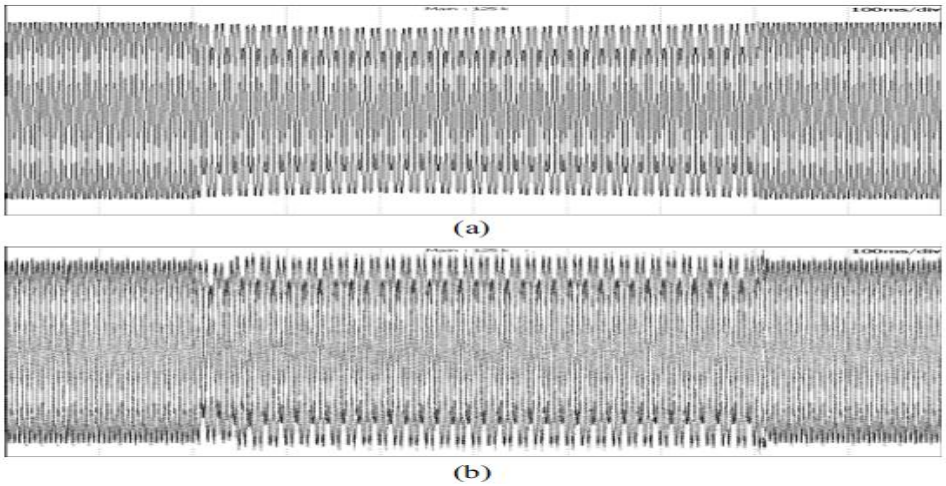

Fig. 17. PCC phase voltages (50 V/div) during the variable profile type I sag. (a)When the control is inactive, (b) when the voltage support control is activated during the sag. (100 ms/div).

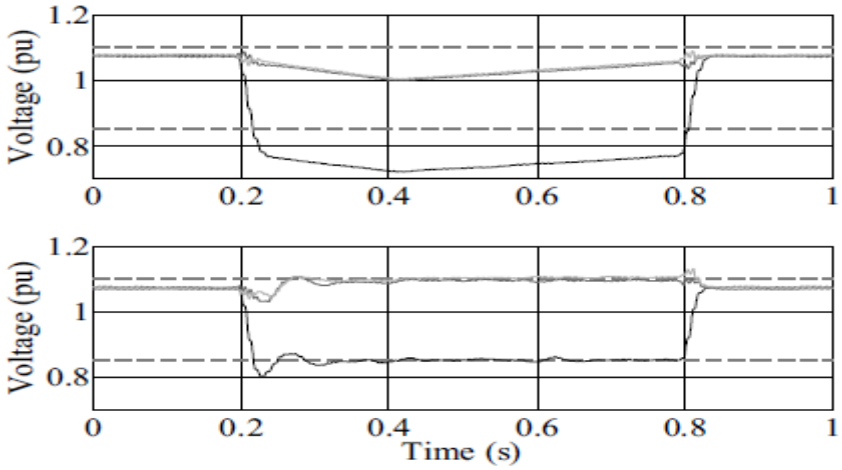

Fig. 18. PCC phase voltages during the type I variable profile sag, without (top) and with voltage support (bottom).

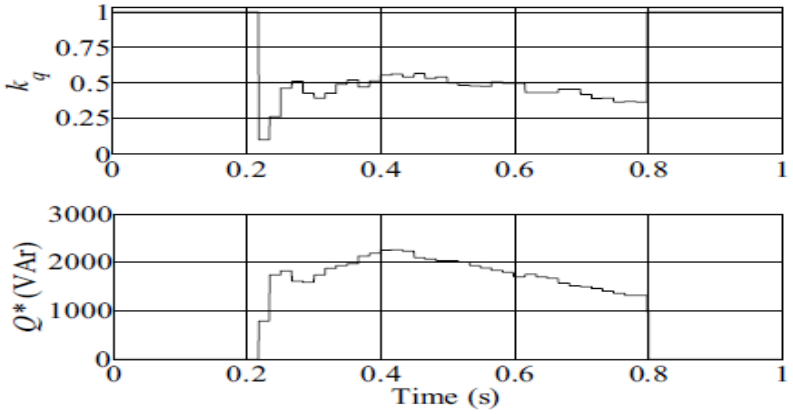

Fig. 19. Control parameter *kq* and reference value of reactive power$Q*$ during the type I variable profile sag.

V. CONCLUSION

This paper has presented a voltage support controller for three-phase grid-connected inverters operating under voltage sags. A detailed mathematical analysis of the injected currents during the voltage sag has been carried out in order to develop the proposed control. It sets two control parameters online: the reactive power reference and a parameter that balances the injection of reactive power via positive and negative sequences. By means of the proposed controller, the inverter helps to restore the droped voltages within the continuous operation limits established by the grid codes. This control strategy has been selected in order to fulfill the desired control objectives by means of low current injection. Analyzing the experimental results, it can be concluded that this proposal may be a good solution to provide voltage support by means of DGS. Further analysis on the performance of the proposed control scheme is open for future research. Particularly, a sensitivity study considering the behavior of the system against variations in power and control parameters should be performed. Also an analysis of the impact of considering variable grid impedance during the fault condition would be of great interest.

REFERENCES

[1]. F. Blaabjerg, R. Teodorescu, M. Liserre, and A. V. Timbus, "Overview of control and grid synchronization for distributed power generation systems," *IEEE Trans. Ind. Electron.*, vol. 53, no. 5, pp. 1398–1409, Oct. 2006.

[2]. S. B. Kjaer, J. K. Pedersen, and F. Blaabjerg, "A review of single-phase grid-connected inverters for photovoltaic modules," *IEEE Trans. Ind. Appl.*, vol. 41, no. 5, pp. 1292–1306, Sep. 2005.

[3]. J. H. Enslin and P. J. Heskes, "Harmonic interaction between a large number of distributed power inverters and the distribution network," *IEEETrans. Power Electron.*, vol. 19, no. 6, pp. 1586–1593, Nov. 2004.

[4]. F. Blaabjerg, Z. Chen, and S. B. Kjaer, "Power electronics as efficient interface in dispersed power generation systems," *IEEE Trans. Power Electron.*, vol. 19, no. 5, pp. 1184–1194, Sep. 2004.

[5]. M. H. J. Bollen, *Understanding Power Quality Problems: Voltage Sags and Interruptions*. New York, NY, USA: IEEE Press, 2000.

[6]. M. Mohseni, S. M. Islam, and M. A. S. Masoum, "Impacts of voltage sags on DFIG-based wind turbines considering phase-angle jump, voltage recovery, and sag parameters," *IEEE Trans. Power Electron.*, vol. 26, no. 5, pp. 1587–1598, May 2011.

[7]. M. H. J. Bollen, "Algorithms for characterizing measured three-phase unbalanced voltage dips," *IEEE Trans. Power Delivery*, vol. 18, no. 3, pp. 937–944, Jul. 2003.

[8]. S. Cundeva, R. Neumann, M. Bollen, Z. Kokolanski, J. Vuletic, A. Krkoleva, S. Djokic, K. van Reusel, and Kurt Stockman, "Immunity against voltage dips – Main recommendations to stakeholders of the CIGRE/CIRED/UIE JointWorking Group C4.110," *Int. J. Emerging Sci.*, vol. 1, pp. 555–563, Dec. 2011.

[9]. L. Zhang, P. Loh, and F. Gao, "An integrated nine-switch power conditioner for power quality enhancement and voltage sag mitigation," *IEEE Trans. Power Electron.*, vol. 27, no. 3, pp. 1177–1190, Mar. 2012.

[10]. J. Miret, M. Castilla, A. Camacho, L. Vicu˜na, and J. Matas, "Control scheme for photovoltaic three-phase inverters to minimize peak currents during unbalanced grid-voltage sags," *IEEE Trans. Power Electron*, vol. 27, no. 10, pp. 4262–4271, Oct. 2012.

[11]. G. Yalc¸inkaya, M. H. J. Bollen, and P. A. Crossley, "Characterization of voltage sags in industrial distribution systems," *IEEE Trans. Ind. Appl.*, vol. 34, no. 4, pp. 682–688, Jul./Aug. 1998.
[12]. "Characteristics of the utility interface for photovoltaic systems," *IEC Standard 61727-2004*, 2004.
[13]. *IEEE Application Guide for IEEE Std 1547, IEEE Standard for Interconnecting Distributed Resources with Electric Power Systems*, IEEE Standard 1547.2-2008, 2009.
[14]. M. Altin, O. Goksu, R. Teodorescu, P. Rodriguez, B.-B. Jensen, and L. Helle, "Overview of recent grid codes for wind power integration," in *Proc. 12th Int. Conf. Optimization Elect. Electron. Equipment*, May 2010, pp. 1152–1160.
[15]. A. Yazdani and R. Iravani, *Voltage-sourced Converters in Power Systems*. New Jersey, USA: Wiley, 2010.
[16]. V. Khadkikar and A. Chandra, "UPQC-S:Anovel concept of simultaneous voltage sag/swell and load reactive power compensations utilizing series inverter of UPQC," *IEEE Trans. Power Electron.*, vol. 26, no. 9, pp. 2414– 2425, Sep. 2011.
[17]. T.-L. Lee, S.-H. Hu, and Y.-H. Chan, "D-STATCOM with positive sequence admittance and negative-sequence conductance to mitigate voltage fluctuations in high-level penetration of distributed generation systems," *IEEE Trans. Ind. Electron.*, vol. 60, no. 4, pp. 1417–1428, Feb. 2013.
[18]. Y. A.-R. I. Mohamed and E. F. El-Saadany, "A control scheme for PWM voltage-source distributed-generation inverters for fast load-voltage regulation and effective mitigation of unbalanced voltage disturbances," *IEEE Trans. Ind. Electron.*, vol. 55, no. 5, pp. 2072–2084, May 2008.
[19]. F.Wang, J. L. Duarte, and M. A. M. Hendrix, "Grid-interfacing converter systemswith enhanced voltage quality formicrogrid application—concept and implementation," *IEEE Trans. Power Electron.*, vol. 26, no. 12, pp. 3501–3513, Dec. 2011.
[20]. A. Junyent-Ferre, O. Gomis-Bellmunt, T. C. Green, and D. E. Soto- Sanchez, "Current control reference calculation issues for the operation of renewable source grid interface VSCs under unbalanced voltage sags," *IEEE Trans. Power Electron.*, vol. 26, no. 12, pp. 3744–3753, Dec. 2011.
[21]. I. Etxeberria-Otadui, U. Viscarret, M. Caballero, A. Rufer, and S. Bacha, "New optimized PWM VSC control structures and strategies under unbalanced voltage transients," *IEEE Trans. Ind. Electron.*, vol. 54, no. 5, pp. 2902–2914, Oct. 2007.
[22]. F. Wang, J. L. Duarte, and M. A. M. Hendrix, "Pliant active and reactive power control for grid-interactive converters under unbalanced voltage dips," *IEEE Trans. Power Electron.*, vol. 26, no. 5, pp. 1511–1521, May 2011.
[23]. A. Camacho, M. Castilla, J. Miret, J. C. Vasquez, and E. Alarcon-Gallo, "Flexible voltage support control for three phase distributed generation inverters under grid fault," *IEEE Trans. Ind. Electron.*, vol. 60, no. 4, pp. 1429–1441, Apr. 2013.
[24]. E. Figueres, G. Garcera, J. Sandia, F. Gonzalez-Espin, and J. C. Rubio, "Sensitivity study of the dynamics of three-phase photovoltaic inverters with an LCL grid filter," *IEEE Trans. Ind. Electron.*, vol. 56, no. 3, pp. 706– 717, Mar. 2009.
[25]. D. N. Zmood, D. G. Holmes, and G. H. Bode, "Frequency-domain analysis of three-phase linear current regulators," *IEEE Trans. Ind. Appl.*, vol. 37, no. 2, pp. 601–610, Mar./Apr. 2001.
[26]. A. K. Abdelsalam, A. M. Massoud, S. Ahmed, and P. N. Enjeti, "High-performance adaptive perturb and observe MPPT technique for photovoltaic-based microgrids," *IEEE Trans. Power Electron.*, vol. 26, no. 4, pp. 1010–1021, Apr. 2011.
[27]. D. Jingya, X. D. Xu, W. B. Wu, and R. R. Zargari, "Unified DC-link current control for low-voltage ride-through in current-source-converterbased wind energy conversion systems," *IEEE Trans. Power Electron.*, vol. 26, no. 1, pp. 288–297, Jan. 2011.
[28]. V. Ignatova, P. Granjon, and S. Bacha, "Space vector method for voltage dips and swells analysis," *IEEE Trans. Power Del.*, vol. 24, no. 4, pp. 2054– 2061, Oct. 2009.
[29]. P. Rodriguez, R. Teodorescu, I. Candela, A. V. Timbus, and F. Blaabjerg, "New positive-voltage sequence detector for grid synchronization of power converters under faulty grid conditions," in *Proc. IEEE 37th Power Electron. Spec. Conf.*, 2006, pp. 1–7.
[30]. H. Akagi, Y. Kanazawa, and A. Nabae, "Instantaneous reactive power compensator comprising switching devices without energy storage components," *IEEE Trans. Ind. Appl.*, vol. IA-20, no. 3, pp. 625–630, May 1984.
[31]. P. Rodriguez, A. V. Timbus, R. Teodorescu, M. Liserre, and F. Blaabjerg, "Flexible active power control of distributed power generation systems during grid faults," *IEEE Trans. Ind. Electron.*, vol. 54, no. 5, pp. 2583– 2592, Oct. 2007.

[32]. L. Asiminoaei, R. Teodorescu, F. Blaabjerg, and U. Borup, "A digital controlled PV inverter with grid impedance estimation for ENS detection," *IEEE Trans. Power Electron.*, vol. 20, no. 11, pp. 1480–1490, Nov. 2005.

[33]. D. N. Zmood, D. G. Holmes, and G. H. Bode, "Frequency-domain analysis of three-phase linear current regulators," *IEEE Trans. Ind. Appl.*, vol. 37, no. 2, pp. 601–610, Mar./Apr. 2001.

[34]. F. J. Rodriguez, E. Bueno, M. Aredes, L. G. B. Rolim, F. A. S. Neves, and M. C. Cavalcanti, "Discrete-time implementation of second order generalized integrators for grid converters," in *Proc. IEEE 34th Ann. Conf. Ind. Electron.*, 2008, pp. 176–181.

[35]. M. Liserre, R. Teodorescu, and F. Blaabjerg, "Stability of photovoltaic and wind turbine grid-connected inverters for a large set of grid impedance values," *IEEE Trans. Power Electron.*, vol. 21, no. 1, pp. 263–272, Jan.2006.